

Rotational directionality via symmetry-breaking in an electrostatic motor

A Celestino¹, A Croy¹, M W Beims^{2,1}, A Eisfeld¹

¹ Max Planck Institute for the Physics of Complex Systems, Nöthnitzer Str. 38, 01187 Dresden, Germany

² Departamento de Física, Universidade Federal do Paraná, 81531-980 Curitiba, Brazil

E-mail: eisfeld@pks.mpg.de

October 14, 2018

Abstract. We theoretically investigate how one can achieve a preferred rotational direction for the case of a simple electrostatic motor. The motor is composed by a rotor and two electronic reservoirs. Electronic islands on the rotor can exchange electrons with the reservoirs. An electrostatic field exerts a force on the occupied islands. The charge dynamics and the electrostatic field drive rotations of the rotor. Coupling to an environment lead to damping on the rotational degree of freedom. We use two different approaches to the charge dynamics in the electronic islands: hopping process and mean-field. The hopping process approach takes into account charge fluctuations, which can appear along Coulomb blockade effects in nanoscale systems. The mean-field approach neglects the charge fluctuations on the islands, which is typically suitable for larger systems. We show that for a system described by the mean-field equations one can in principle prepare initial conditions to obtain a desired rotational direction. In contrast, this is not possible in the stochastic description. However, for both cases one can achieve rotational directionality by changing the geometry of the rotor. By scanning the space formed by the relevant geometric parameters we find optimal geometries, while fixing the dissipation and driving parameters. Remarkably, in the hopping process approach perfect rotational directionality is possible for a large range of geometries.

PACS numbers: 85.35.-p, 85.75.-j

Keywords: Symmetry breaking, rotors, electrostatic motor, rotational directionality, unidirectional rotation

Submitted to: *New J. Phys.*

1. Introduction

Rotary motors are paradigmatic devices which transform input energies in controlled rotations. These rotations can be employed to yield work, powering a nanomachine for instance [1, 2]. In the micro-scale these devices have been assembled with nanowires [3, 4] and microfabricated gears [5]. Since the advent of the first synthetic molecular motor [6, 7], many different designs for nano-scale motors were proposed [8, 9, 10, 11, 12, 13] and realized [14, 15, 16, 17, 18, 19, 20, 21]. Significant steps towards application of rotary motors have been made, for instance they have been used to propel a molecule in a Cu(111) surface [22], rotate microscale objects [23] and control chemical reactions [24]. These devices can be driven in many different ways, using e.g. light [6, 16, 5], chemical energy [7, 25], electronic current [17, 20, 21] and electric fields [15, 3]. Recent publications [11, 12, 13] consider single-electron tunnelling to drive a nanoelectromechanical rotor. In the present work, we will focus on the setup of Ref. [11]. In this setup, sketched in figure 1, a mechanical rotor is placed between two leads at different chemical potentials. The rotor has islands (capacitors) attached to its tips and electrons can tunnel from the “source” lead to the islands and from the islands to the “drain” lead. An electrostatic field between the leads induces a force on the charged islands, which eventually leads to a torque on the rotor.

The charging and discharging processes depend fundamentally on the size of the islands, and consequently on the size of the device. For nano-scale devices where the Coloumb blockade plays a role, the islands can only host a small number of electrons (in the extreme case only one). In this case, charge fluctuations caused by the stochastic nature of the tunnelling process lead to torque fluctuations on the rotor. On the other hand, for larger devices where Coulomb blockade is not relevant, charge fluctuations are irrelevant, since they are very small compared to the mean charge on the islands. In Ref. [11] it has been discussed that a mean-field description, which is valid for macroscopic rotors, is also able to reproduce certain aspects of the stochastic description which describes rotors in the Coulomb blockade regime. In particular, it has been found that by increasing the ratio of the driving and damping parameters one obtains a regime where the rotor is performing rotational motion and the (averaged) angular momentum is the same in the stochastic and the mean field description.

For many applications it is crucial to attain control over the directionality of the rotations of the motor. In the mean-field description, the rotational direction depends on the specific initial condition (IC). The IC is characterized by the initial angular momentum $L(t = 0) = L_0$, the initial angle $\theta(t = 0) = \theta_0$, and the initial electronic charges $Q_A(t = 0)$ and $Q_B(t = 0)$ on the islands. However, the experimental preparation of a specific IC can be difficult, imprecise or even inconvenient, depending on the system scale, suppression of noise-sources, etc. Moreover, imperfections in the rotor fabrication, namely in the length of its arms, angle between them, capacities of the islands, etc. could also lead to uncertainty over the rotational direction. In the stochastic description the rotation direction can either vary from realization to realization independently of the IC

(weak electric field, strong damping), or even alternate in time within a single trajectory (strong electric field, weak damping).

Another way of attaining rotational directionality is to make a rotation direction “preferable”. With “preferred direction” we mean that most of, or even all ICs(realizations) lead to rotations in this direction. For a perfectly symmetric rotor, it is intuitively clear that no directionality is achieved: for each IC(realization) leading to a certain rotation direction there exists another one leading to the opposite direction. This gives rise to the question which symmetries of the rotor one has to break in order to achieve directionality of the rotatory motion.

In this paper, we show that by changing simultaneously the angle between the arms of the rotor and their length, it is possible to introduce a preferred direction of rotation. We search in particular for combinations of the parameters which lead to directional rotatory motion. We will also see that it is not sufficient to change either the angle or the length alone. The parameter space of the studied system presents regions where all ICs end up rotating in the same direction and with the same $L(t)$. It means that no control over IC is required to achieve a certain direction of rotation, and that within some constraints, the rotor fabrication can also present imperfections.

The paper is organized as follows. Section 2 presents the model for the electrostatic motor, which includes the mean-field equations of motion, and discussions about relevant quantities. While Sec. 3 presents some features of the symmetric rotor, Sec. 4 shows how directional rotatory motion can be achieved in the mean-field approach. In Sec. 5 we treat the case of nanoscale devices using a hopping-process approach for the tunnelling and in Sec. 6 we summarize our results.

2. Mean-field equations and definitions

In this section we present mean-field equations of motion for the rotor, discuss as special example the symmetric rotor, and provide definitions of several quantities which will be of interest in the following sections.

2.1. Mean-field equations of motion

We consider a rotor composed of insulating arms and electronic islands A and B placed at their ends as sketched in figure 1. The rotor is immersed in a region with a homogeneous, time-independent electric field \mathbf{E} , directed along the horizontal axis. To specify the orientation of the rotor, we use the angle θ between the rotor arm connected to A and the horizontal line as indicated in figure 1. We allow the two arms of the rotor to be tilted with respect to each other, and denote the angle between them by β . The islands can host charges Q_A and Q_B up to a certain limit Q_{\max} (chosen to be equal for both islands) which is given by their capacitances $C_A = C_B$. As in Ref. [11], we start by considering the dynamics using a mean-field approach where charge fluctuations are neglected and the charge dynamics is purely deterministic. This mean-field allows

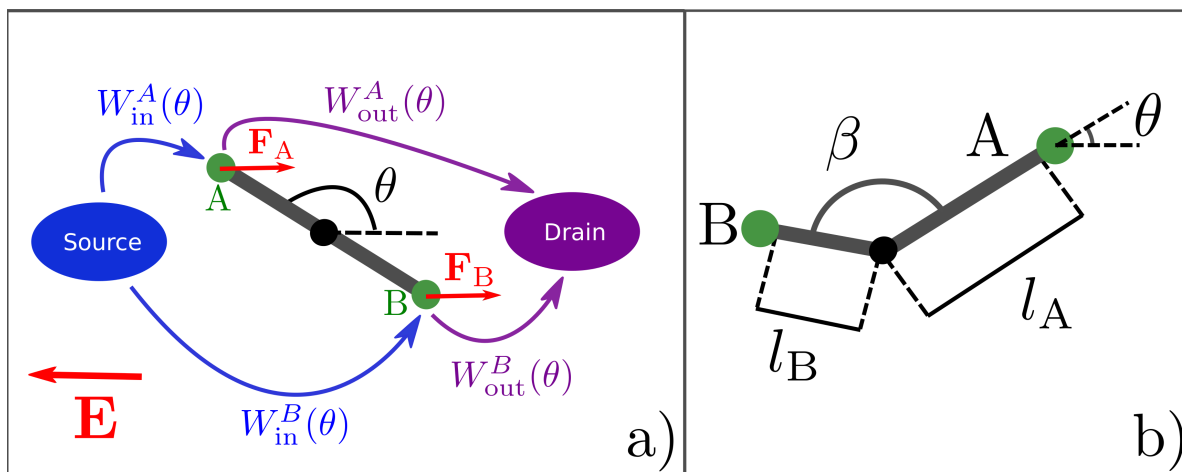


Figure 1: Sketch of the setup and its relevant parameters. The setup is composed by a rotor (shaft, arms and islands A and B) and two negative charge reservoirs (source and drain). The rotor's orientation is given by θ . The islands A and B are (dis)charged by the source with rate $W_{\text{in}}^{A/B}$ ($W_{\text{out}}^{A/B}$). An electrostatic field \vec{E} exerts a force \vec{F} on the charged islands. While in a) the *symmetric* rotor is shown, in b) the *asymmetric* rotor is displayed together with the parameters to describe the deviation from the symmetric case.

one already to understand the fundamentals of the symmetry-breaking and is strictly valid for macroscopic devices (see Appendix Appendix B). The hopping-process for the tunneling, which is more suitable to nanoelectromechanical devices, will be considered in Section 5. The equations that describe the charge dynamics on the islands in the mean-field they are given by

$$\frac{dQ_A}{dt} = W_{\text{in}}(\theta)(Q_{\text{max}} - Q_A) - W_{\text{out}}(\theta)Q_A, \quad (1a)$$

$$\frac{dQ_B}{dt} = W_{\text{in}}(\theta + \beta)(Q_{\text{max}} - Q_B) - W_{\text{out}}(\theta + \beta)Q_B, \quad (1b)$$

where t is time, $W_{\text{in}}(\theta')$ and $W_{\text{out}}(\theta')$ are charging and discharging rates, respectively, and their argument $\theta' = \theta$ for the island A and $\theta' = \theta + \beta$ for the island B. We assume $W_{\text{in/out}}(\theta)$ to be positive even functions (their functional dependence on the angles θ and $\theta + \beta$ is going to be specified in subsection 2.3). In the following we use dimensionless quantities. We define $\tau = t/t_0$ (t_0 is a characteristic time-scale for the electronic dynamics), $q_A(t) = Q_A(t)/Q_{\text{max}}$ and $q_B(t) = Q_B(t)/Q_{\text{max}}$ and $w_{\text{in/out}}(\theta') = t_0 W_{\text{in/out}}(\theta')$. Then the dimensionless version of equations (1a) and (1b) is

$$\frac{dq_A}{d\tau} = w_{\text{in}}(\theta)(1 - q_A) - w_{\text{out}}(\theta)q_A, \quad (2a)$$

$$\frac{dq_B}{d\tau} = w_{\text{in}}(\theta + \beta)(1 - q_B) - w_{\text{out}}(\theta + \beta)q_B. \quad (2b)$$

To realize these mean-field equations experimentally one can use for example RC circuits, where the islands are capacitors. Their capacitances have an angle dependence

Table 1: Dimensionless quantities and their definitions.

Quantity	Symbol	Formula
Time	τ	$\frac{t}{t_0}$
Charge	$q_{A/B}$	$\frac{Q_{A/B}}{Q_{\max}}$
Charging rate	$w_{\text{in/out}}(\theta)$	$t_0 W_{\text{in/out}}(\theta)$
Angular momentum	Λ	$\frac{t_0 L}{I}$
Asymmetry parameter	χ	$\arctan\left(\frac{l_A}{l_B}\right)$
Driving strength	η_0	$\sqrt{\frac{l_A^2 + l_B^2}{2}} \left[\frac{t_0^2 Q_{\max} E}{I} \right]$

$C_A(\theta) = [R(W_{\text{in}}(\theta) + W_{\text{out}}(\theta))]^{-1}$ and $C_B(\theta) = [R(W_{\text{in}}(\theta + \beta) + W_{\text{out}}(\theta + \beta))]^{-1}$, where R is the resistance (details are given in appendix Appendix B).

Since the rotor is placed within an electric field, the islands experience a force when they are charged. Within the mean-field approach one finds the following set of coupled equations for the dynamics of the mechanical degrees of freedom (For a derivation we refer to appendix Appendix A)

$$\frac{\partial}{\partial \tau} \Lambda = -\eta_0 \sqrt{2} (\sin \chi \sin(\theta) q_A + \cos \chi \sin(\theta + \beta) q_B) - \gamma \Lambda, \quad (3a)$$

$$\frac{\partial}{\partial \tau} \theta = \Lambda. \quad (3b)$$

Here, we have introduced the dimensionless angular momentum $\Lambda = t_0 L / I$, where L is the actual angular momentum and I is the moment of inertia of the rotor. The asymmetry parameter $\chi \in [0, \pi/2]$ is given by $\tan \chi = l_A / l_B$, with $l_{A(B)}$ being the length of the arm containing island A(B). The driving strength $\eta_0 > 0$ is

$$\eta_0 = \sqrt{\frac{l_A^2 + l_B^2}{2}} \left[\frac{t_0^2 |Q_{\max}| E}{I} \right], \quad (4)$$

with $E = |\vec{E}|$ being the electric field strength. A surrounding environment leads to the phenomenological damping-term, whose strength is given by the dimensionless viscosity parameter γ . The dimensionless quantities can be seen in Table 1.

Note that $q_A(t)$ and $q_B(t)$ are determined by equations (2a) and (2b). Since the right hand side of equations (2a) and (2b) depends on the angle θ we have to solve the non-linear system of coupled equations (2a)-(3b).

2.2. Quantities of interest

We are interested in the influence of initial conditions on the steady-state behavior of the system. In particular we are interested in the time-average of the angular momentum (sign and magnitude) and charge current. The time-averaged angular momentum is defined as

$$\langle \Lambda \rangle = \frac{1}{\mathcal{T} - \tau_{\text{tran}}} \int_{\tau_{\text{tran}}}^{\mathcal{T}} \Lambda(\tau) d\tau, \quad (5)$$

where τ_{tran} is a typical transient time ‡ and \mathcal{T} is sufficiently large to make $\langle \Lambda \rangle$ reach its stationary value.

We also investigate the time-averaged electronic current that flows through the system, and its dependence on the ICs. The dimensionless time-averaged current is defined as

$$\langle J \rangle = \frac{1}{\mathcal{T} - \tau_{\text{tran}}} \int_{\tau_{\text{tran}}}^{\mathcal{T}} [w_{\text{out}}(\theta(\tau))q_A(\tau) + w_{\text{out}}(\theta(\tau) + \beta)q_B(\tau)]d\tau, \quad (6)$$

and the physical current is then given by $\langle J \rangle Q_{\text{max}}/t_0$. Again, we consider the same transient-time τ_{tran} as in equation (5) and \mathcal{T} to be large enough such that $\langle J \rangle$ reaches its stationary value after \mathcal{T} . In order to calculate $\langle \Lambda \rangle$ and $\langle J \rangle$ we solve the set of equations (2a)-(3b) numerically, and use the trajectories to calculate the time-integrals (5) and (6).

2.3. Specific form of the (dis)charging rates

Although our discussion does not require any specific form of $w_{\text{in/out}}(\theta')$ we will use as an example the functional form adopted in Ref. [11] to describe a nano-scale electromechanical rotor, namely

$$w_{\text{in}}(\theta') = e^{-\xi \cos(\theta')}, \quad (7a)$$

$$w_{\text{out}}(\theta') = e^{\xi \cos(\theta')}. \quad (7b)$$

In Ref. [11] this particular form of $w_{\text{in/out}}(\theta')$ stems from the exponentially decreasing (with respect to the lead-island distance) tunneling rates §. In this work we will take ξ to be identical for the two islands and for source and drain. ||

3. Symmetric rotor

For reference, we start with the dynamics of the symmetric rotor ($\beta = \pi$ and $\chi = \pi/4$), which has aligned arms with the same length ($l_A = l_B$). From now on, we will consider the charge IC $q_A(\tau=0) = q_B(\tau=0) = 0$.

‡ In deterministic systems it is well defined that a dissipative system needs a certain time τ_{tran} [depending on the initial conditions] to reach with a certain precision an asymptotic manifold in phase space called attractor [26]. For systems described by stochastic differential equations one still has the concept of transient-time, although the concept of attractors as asymptotic manifolds in phase space becomes meaningless [27].

§ In the nanoscale realization the dimensionless parameter ξ is related to the so-called tunneling length λ by $\xi = l/\lambda$, where $l = l_{A,B}$ is the length of the arm attached to A or B [11], as one can identify in figure 1. The tunneling length is determined mainly by the choice of materials used to build the leads as well as the systems implemented as islands implementation.

|| Since $l = l_{A,B}$ is the length of the rotor's arms, one sees immediately that one needs specific tunneling lengths $\lambda_{A,B}$ in order to keep ξ independent on the considered island. This could be done, for instance, using different materials for the islands.

3.1. Invariances of the symmetric rotor

In the case of the symmetric rotor, solutions of the coupled equations (2a)-(3b) possess the following invariance: Substituting $\tilde{\Lambda} = -\Lambda$ and $\tilde{\theta} = -\theta$ *simultaneously* in equations (2a)-(3b), i.e. changing the direction of rotation and reflecting around $\theta = 0$, one obtains the same equation. This invariance (with the rotation inversion) occurs also for reflections around $\theta = \pi/2$ and around $\theta = 3\pi/2$. Due to these invariances, for every counter-clockwise (positive Λ) rotating solution with initial condition (Λ_0, θ_0) there is another clockwise (negative Λ) rotating one with initial condition $(-\Lambda_0, -\theta_0)$. This invariance will be of fundamental importance when we consider the time-averaged angular momentum $\langle \Lambda \rangle$, which is a function of the IC, averaged over θ_0 for a rotor initially discharged ($q_A(\tau=0) = q_B(\tau=0) = 0$) and at rest ($\Lambda_0 = 0$)

$$\overline{\langle \Lambda \rangle} = \frac{1}{2\pi} \int_0^{2\pi} d\theta_0 \langle \Lambda \rangle, \quad (8)$$

which becomes exactly zero in the presence of this invariance.

3.2. IC-space of the symmetric rotor

It turns out that the steady-state dynamics depends sensitively on the ratio η_0/γ [11]. For a given ξ one has three dynamical regimes: for very small η_0/γ there is no motion at all and the rotor rests in the position $\theta = \pi/2$. For larger η_0/γ there is an interval where oscillations are found. Above a certain threshold of η_0/γ rotational motion sets in where the angular momentum increases approximately as the square root of η_0/γ . As said before, here we focus on parameters where rotational motion occurs and we will consider the case $\xi = 2$ as an example.

Figure 2 compares the behavior for two values of η_0/γ . Red stands for clockwise (negative Λ) and blue for counter-clockwise (positive Λ) rotation direction. Throughout the IC-space, for both negative and positive $\langle \Lambda \rangle$, one has the same $|\langle \Lambda \rangle|$. In both plots one observes intertwined patterns spiraling towards $(\theta_0 = \pi/2, \Lambda_0 = 0)$ and $(\theta_0 = 3\pi/2, \Lambda_0 = 0)$. These points correspond to the standstill situation ($\Lambda = 0$) with the rotor in a vertical orientation. Both locations are fixed points in phase space: Once the system reaches those states, it stays there forever. The spiraling pattern around these fixed points can be understood as follows: the rotor transiently oscillates and as it swings it gains energy until it reaches the rotatory steady-state. In each half oscillation the rotor has the chance to set into the rotatory steady-state with a certain rotation direction. If it does not have enough energy, it performs another half oscillation gaining more energy and having the opportunity to start rotating into the opposite direction. This process is repeated until the stationary rotatory state is reached, whose direction depends on the IC of the rotor. For ICs closer to the fixed points a larger number of oscillations is required to reach the steady-state and small changes of the IC can lead to a different direction of rotation. This fact causes the complex spiraling pattern seen in the figures. As one decreases the driving strength η_0 the rotor gains energy more slowly

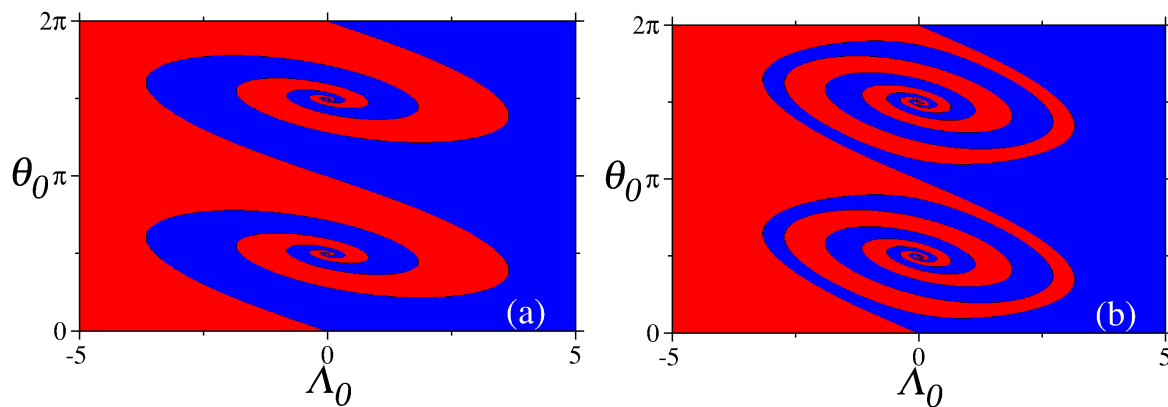


Figure 2: Time averaged angular momentum (color) $\langle \Lambda \rangle$ as a function of the ICs (Λ_0, Θ_0) for $q_A(\tau=0) = q_B(\tau=0) = 0$, $\xi = 2.0$, $\gamma = 1$ and (a) $\eta_0/\gamma = 10.0$ (b) $\eta_0/\gamma = 5.0$. Red stands for clockwise (negative Λ) and blue for counter-clockwise (positive Λ) rotation direction.

and therefore more and more oscillations are required in order to reach the rotatory regime, which in turn leads also to finer spiraling patterns, as one sees in figure 2 (b).

In figure 2 one can also see a consequence of the invariance discussed above in subsection 3.1, namely an anti-symmetry around $\theta_0 = 0$ ($\theta_0 = \pi$) and $\theta_0 = \pi/2$ ($\theta_0 = 3\pi/2$) and $\Lambda_0 = 0$. This anti-symmetry implies in particular that $\overline{\langle \Lambda \rangle} = 0$. In the following section we will show how one can induce a preferred rotation direction, i.e. to make $\overline{\langle \Lambda \rangle} \neq 0$, even in the case when the angular momentum is initially zero.

Now we turn our attention to the second quantity of interest defined in subsection 2.2, namely the time-averaged current $\langle J \rangle$. The time-averaged current only depends on the magnitude (and not on the sign) of the angular momentum. Therefore all ICs lead to the same time-averaged current and we do not present a plot of $\langle J \rangle$ as a function of the ICs (Λ_0, θ_0) .

4. asymmetric rotor

In this section we investigate how one can obtain $\overline{\langle \Lambda \rangle} \neq 0$ by breaking the rotor's symmetry.

4.1. Changing either β or χ : No directionality of the rotatory motion

Individual alterations of the parameters β or χ (e.g. just $l_A \neq l_B$) do not lead to a preferred rotational direction, since for every solution $[\theta(t), \Lambda(t)]$ of equations (3a) and (3b) there is another solution $(\tilde{\theta} = -\theta(t) + \phi, \tilde{\Lambda} = -\Lambda(t))$, where ϕ is a fixed angle. Although those changes do not introduce a preferred rotational direction, it is instructive to understand the effects of changing β and χ in equations (3a) and (3b). Examples can be seen in figure 3, where $\langle \Lambda \rangle$ is plotted as a function of the ICs (Λ_0, θ_0) again. Red stands for clockwise (negative Λ) and blue for counter-clockwise (positive

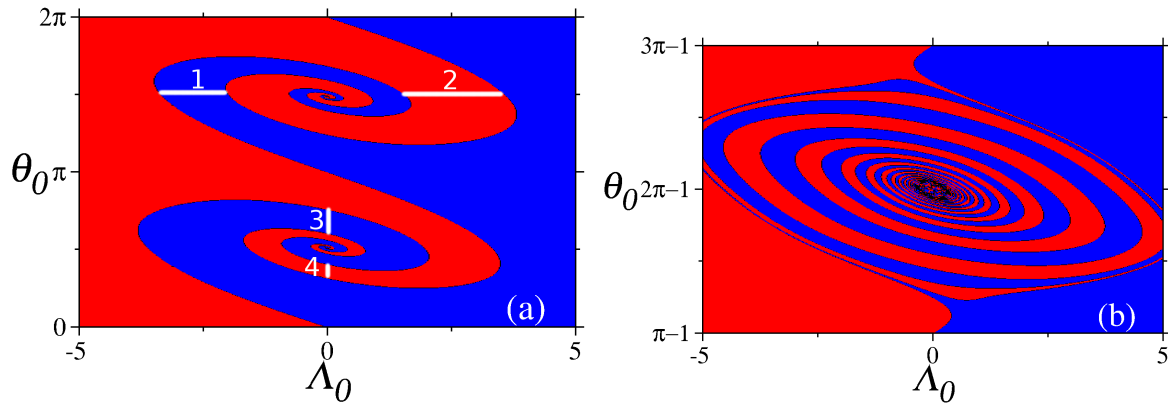


Figure 3: Time averaged angular momentum (color) $\langle \Lambda \rangle$ as a function of the ICs (Λ_0, Θ_0) for $\xi = 2.0$, $\gamma = 1$, $\eta_0 = 10$ and $q_A(\tau=0) = q_B(\tau=0) = 0$. In (a) $\chi = 0.7$ and $\beta = \pi$. Marked with white lines is the width of several regions with the same $\langle \Lambda \rangle$. In (b) $\chi = \pi/4$ and $\beta = 2$ (notice the shifted θ_0 -axis). The color coding is as in figure 2.

Λ) rotational direction. Notice that although $\langle \Lambda \rangle$ changes sign across the IC-space, its absolute value is constant. In figure 3 (a) one sees the case $l_A \neq l_B$ ($\chi \neq \pi/4$) and $\beta = \pi$, while in b) the case $l_A = l_B$ ($\chi = \pi/4$) and $\beta = 2$ is shown. The figure 3 (a) looks qualitatively similar to figure 2 (a) and (b). Again, one has fixed points (the same as for the symmetric rotor) and a patterned structure that spirals towards them. Nevertheless, the point anti-symmetry around the fixed points $\theta = \pi/2$ and $\theta = 3\pi/2$ ($\Lambda = 0$) is no longer present. This can be seen by comparing the lengths of the line segments 1 and 2 (3 and 4) in figure 3 (a), which are the widths of regions with the same $\langle \Lambda \rangle$ measured symmetrically with respect to the aforementioned fixed points. The point anti-symmetry around the fixed points $\theta = 0$ and $\theta = \pi$ is preserved though. Figure 3 (b) presents other differences when compared to figure 2 (a) and (b): Two fixed points disappear and other two are localized at different positions, namely $\theta = 2\pi - \beta/2$ and $\theta = \pi - \beta/2$. Nevertheless, the IC-space is still point anti-symmetric with respect to the fixed point positions, and therefore again one has $\overline{\langle \Lambda \rangle} = 0$. The complete breakage of these point anti-symmetries is just possible by setting both $\chi \neq \pi/4$ and $\beta \neq \pi$, and it is exactly this symmetry-breaking that will be exploited to generate directed rotational motion in the next section.

4.2. Changing both β and χ : directionality of the rotatory motion

In order to obtain a preferred rotational direction one needs to modify $l_A \neq l_B$ ($\chi \neq \pi/4$) and $\beta \neq \pi$ simultaneously. The resulting set of equations does not feature pairs of solutions $(\theta(t), \Lambda(t))$ and $(\theta'(t), \Lambda'(t))$ such that $\theta'(t) = -\theta(t) + \phi$ and $\Lambda'(t) = -\Lambda(t)$.

To quantify the resulting directionality of the rotatory motion we define a

directionality measure in the IC-space

$$M = \frac{\overline{\langle \Lambda \rangle}}{\sqrt{\overline{\langle \Lambda \rangle^2}}}, \quad (9)$$

where the overbar was defined in equation (8). Note that M is zero when $\overline{\langle \Lambda \rangle} = 0$. For the case where all the θ_0 lead to rotation in the same direction (and with the same angular velocity) one has $M = \pm 1$. By changing from negative to positive values of M (or vice-versa), we just change the direction of rotation.

The figure 4 shows M as a function of the parameters β and χ . Black indicates no rotational directionality, while from blue(red) to cyan(yellow) an increasing value of the directionality measure is found, with a positive(negative) $\overline{\langle \Lambda \rangle}$. In figure 4 we set the parameter $\gamma = 1$ and vary η_0 (in a) to c)). Along the two lines $\beta = \pi$ and $\chi = \pi/4$ we have $M = 0$, as expected. The M values are also anti-symmetric about those lines and, consequently, point-symmetric with respect to $(\chi = \pi/4, \beta = \pi)$. This point-symmetry stems from the analytic form in which the parameters χ and β appear into equation (3a), and therefore it is present independently of the chosen γ and η_0 (and ξ). In figure 4 a) ($\eta_0/\gamma = 5$) and b) ($\eta_0/\gamma = 10$) there are regions with $|M| = 1$, in which a total rotational directionality is achieved. For instance, the point C in figure 4 b) has $M = 1$. In this case all the ICs lead to the same direction and magnitude of rotation (even for large $|\Lambda_0|$). However, in figure 4 a) almost all the parameter space presents $M = 0$, since for such small ratio η_0/γ the rotor has $\langle \Lambda \rangle = 0$ for most of the (χ, β) values. Regions where $|M| < 1$ are also displayed in figure 4 b) and c) ($\eta_0/\gamma = 30$). Interestingly, figure 4 c) presents no $|M| = 1$ regions, although larger extensions of the parameter space have $|M| > 0$. No significant changes in these figures are verified when $\xi = 1$ or $\xi = 4$.

Examples for the cases $1 > |M| > 0$ are the points A and B. For these points we generate the IC-space of figure 5. In figure 5 (a)((b)) we plot $\langle \Lambda \rangle$ in the IC-space for the same parameters as in the point A(B) of figure 4. There, we find $M = 0.47(M = 0.88)$. The white line is drawn in figure 5 just with the purpose of indicating the locus where the IC-average is performed. By comparing the segments of the white line which are inside regions with positive and negative $\langle \Lambda \rangle$ in both figure 5 a) and b), and noting that $|\langle \Lambda \rangle|$ is the same for both red and blue regions, one can understand why the point B presents a stronger rotational directionality than point A in figure 4 b). We do not show a figure with $\langle \Lambda \rangle$ as a function of the ICs for the same parameters as on the point C of figure 4 (b) because *all* the ICs lead to the same $\langle \Lambda \rangle$ value (even for $\Lambda_0 \neq 0$).

5. Nanoscale rotor: Stochastic tunneling

If the size of the rotor (in particular the islands) is shrunk, such that only single electrons are transferred, the mean field description used in Sec. 2 is not suitable. The charge fluctuations can be of the order of the mean values and it is more appropriate to consider the (dis)charging of the islands as a hopping-process. Now the islands can either be

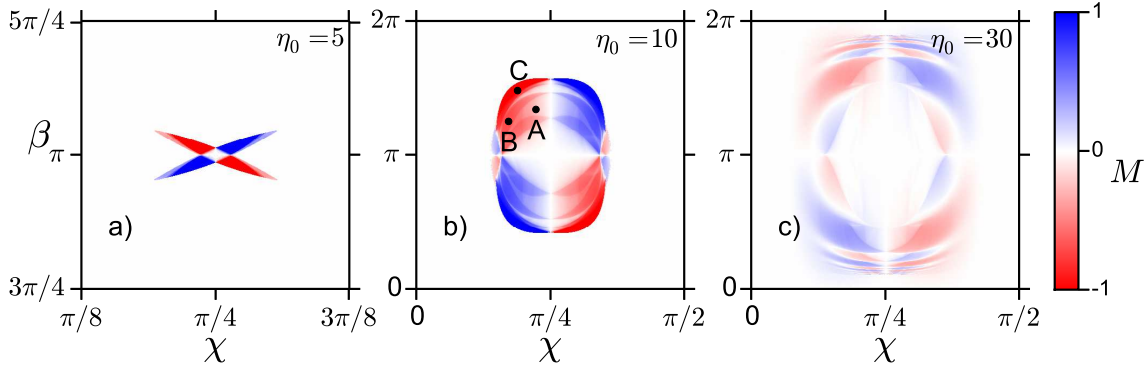


Figure 4: directionality measure M defined in equation (9) as a function of the parameters (χ, β) , for $\xi = 2$ and $\gamma = 1$.

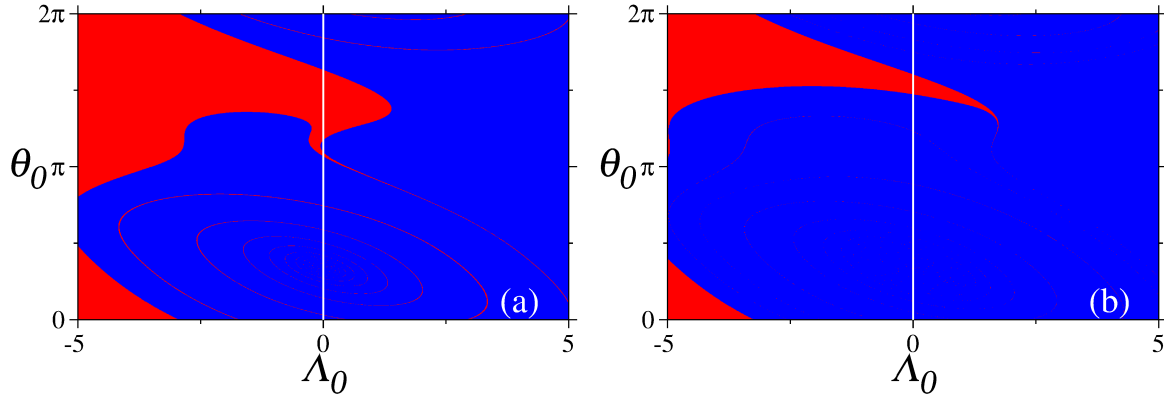


Figure 5: The averaged angular momentum $\langle \Lambda \rangle$ as a function of the ICs (Λ_0, θ_0) for the set of parameters correspondent to a) point A ($\chi = 0.7, \beta = 4.2$), b) point B ($\chi = 0.54, \beta = 3.92$) in figure 4 b). The color coding is as in figure 2. Along the white line in the figures the directionality measure was calculated, as a) $M \approx 0.47$ and b) $M \approx 0.88$.

empty or occupied by one electron, so that the charges Q_A and Q_B can be either 0 or $-e$. The occupation in the islands changes from 0 to $-e$ or vice versa whenever a tunneling event occurs. The tunneling is modeled as a stochastic event. The probability for a tunneling event during an infinitesimal time interval $d\tau$ is

$$dP_{\text{in},i} = d\tau W_{\text{in}}(\theta'), \quad (10a)$$

$$dP_{\text{out},i} = d\tau W_{\text{out}}(\theta'), \quad (10b)$$

where $dP_{\text{in},i}$ ($dP_{\text{out},i}$) is the infinitesimal probability of tunneling in(out) the island $i = A, B$, and $\theta' = \theta$ for $i = A$ and $\theta' = \theta + \beta$ for $i = B$.

In order to assess the impact of this stochastic (dis)charging on the directionality of the rotatory motion we exemplarily calculate directionality measure as a function of the parameters (χ, β) . Since the tunneling is a stochastic process, one needs to redefine the directionality measure. Instead of considering $\langle \Lambda \rangle$ and $\langle \Lambda \rangle^2$, we consider their average

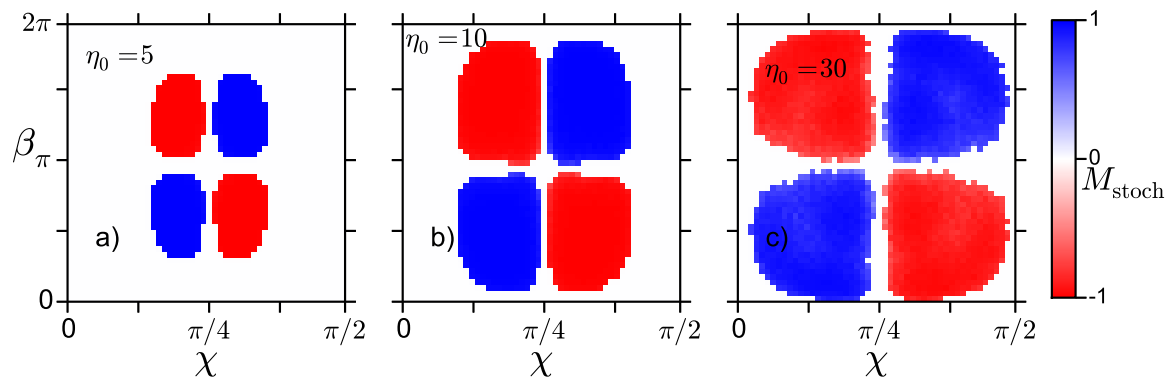


Figure 6: Directionality measure M_{stoch} defined in equation (11) as a function of the parameters (χ, β) , for $\xi = 2$ and $\gamma = 1$ (same parameter set and color coding as in figure 4).

over the realizations $\langle\langle\Lambda\rangle\rangle_{\text{re}}$ and $\langle\langle\Lambda\rangle\rangle_{\text{re}}^2$, such that the new directionality measure is

$$M_{\text{stoch}} = \frac{\overline{\langle\langle\Lambda\rangle\rangle_{\text{re}}}}{\sqrt{\overline{\langle\langle\Lambda\rangle\rangle_{\text{re}}^2}}}, \quad (11)$$

where $\langle\dots\rangle_{\text{re}}$ is an average over realizations and the overbar the same average over ICs as in equation (9). The directionality measure $M_{\text{stoch}} = 0$ when $\overline{\langle\langle\Lambda\rangle\rangle_{\text{re}}} = 0$. For $M_{\text{stoch}} = \pm 1$ one has *all* ICs leading to net rotations in the same direction with the same $\langle\langle\Lambda\rangle\rangle_{\text{re}}$, such that the sign just indicates the direction of rotation. It must be noted that the sign of $\Lambda(t)$ within a *single trajectory* can change with time, even though we have $M_{\text{stoch}} = \pm 1$.

The figure 6 shows M_{stoch} as a function of the parameters β and χ for the same γ , η_0 and ξ as in figure 4. Black indicates no rotational directionality, while from blue(red) to cyan(yellow) an increasing value of the directionality measure is found, with a positive(negative) $\langle\Lambda\rangle$. M_{stoch} presents the same symmetry in the parameter space as M does. Along the two lines $\beta = \pi$ and $\chi = \pi/4$ we have the expected $M_{\text{stoch}} = 0$ value. The M_{stoch} values are also anti-symmetric about those lines and, consequently, point-symmetric with respect to $(\chi = \pi/4, \beta = \pi)$. Again, this symmetry is independent of the chosen η_0 and γ . The figure 6 features extensive regions of total or partial rotational directionality, namely in the red-yellow and blue-cyan areas. This represents a striking difference to the mean-field equations results from figure 4. The results also do not depend on η_0/γ so sensitively as in the mean-field case (compare figure 6 with figure 4). Nevertheless, the $|\langle\langle\Lambda\rangle\rangle_{\text{re}}|$ achieved are smaller than the typical $\langle\Lambda\rangle$ from the mean-field case. This can be partially explained by the fact that $\Lambda(t)$ can change its sign within a single trajectory.

6. Conclusions

In the present work we have studied how to control the rotational direction of an electromechanical rotor. We describe the charge dynamics in the islands using two different approaches: a mean-field approach, where charge fluctuations are disregarded; and a hopping-process approach, where the charge transfer occurs via stochastic tunneling events. The first approach is valid for a macroscopic electromechanical rotor (see appendix Appendix B), while the second one is more appropriate for a nanoelectromechanical device where the Coulomb blockade effect is relevant.

In the mean-field approach, rotational direction control can be achieved in two different ways: one can either select the rotational direction via choosing an appropriated IC, or one can break the symmetry of the rotor to introduce a preferred rotational direction. In order to experimentally perform the first method in a macroscopic system, the precision of the IC preparation must be high enough to resolve structures in the IC-space. While our mean-field calculations show that increasing the ratio η_0/γ also increases the IC-space size of the structures, through the hopping-process calculations one sees that charge fluctuations can destroy the dependence of the system on the IC. This means that an IC preparation scheme may fail for a real nanoelectromechanical rotor. Apart from that, fabrication imperfections can also spoil the attempts of selecting a specific IC which leads to a certain rotational direction. In contrast, our numeric simulations show that, by breaking the rotor's symmetry, most or even *all* ICs lead to the same rotational direction. For that reason, we focused on the symmetry-breaking procedure.

We have shown that one needs to change the system's parameters χ and β *simultaneously* in order to break the symmetry of the rotor. The parameter β is tuned by setting a tilting angle between the two rotor's arms. We have considered the ratio between the arms' lengths to determine χ , but another way would be having islands with different maximal charges $Q_{\max A/B}$. The parameter space of both mean-field and stochastic equations features extensive areas where a total rotational directionality (with directionality measure modulo 1) is present. In these areas, IC-space scans indicate that the same $\langle \Lambda \rangle (\langle \langle \Lambda \rangle \rangle_{\text{re}})$ in the mean-field(hopping-process) approach is obtained *independently* of the chosen IC. The symmetry-breaking procedure works for large sections of the parameter space. In an experimental realization of our equations, imperfections in the rotor fabrication within the limits of these sections would not spoil the symmetry-breaking. Additionally, our stochastic simulations feature large regions in the parameter space leading to rotational directionality. Thus, this procedure may work specially well for nanoelectromechanical rotors.

Acknowledgments

MWB thanks CNPq (Brazil) for financial support.

Appendix A. Derivation of the mechanical equations of motion

In this section we derive equations (3a) and (3b), which determine the dynamics of the rotor's mechanical degrees of freedom. The torque T that acts on the rotor is given by

$$T = \frac{\partial}{\partial t} L = l_A E Q_A \sin \theta + l_B E Q_B \sin(\theta + \beta) - \lambda L, \quad (\text{A.1})$$

where L is the angular momentum of the rotor. The equation for the angle θ is

$$\frac{\partial}{\partial t} I \theta = L, \quad (\text{A.2})$$

where I is the moment of inertia of the rotor. Dividing equation (A.1) by $Q_{\max} I / t_0^2$ one obtains

$$\frac{\partial}{\partial t / t_0} \left(\frac{L t_0 / I}{Q_{\max}} \right) = \frac{l_A E}{I / t_0^2} \frac{Q_A}{Q_{\max}} \sin \theta + \frac{l_B E}{I / t_0^2} \frac{Q_B}{Q_{\max}} \sin(\theta + \beta) - \frac{\lambda}{I / t_0^2 Q_{\max}} L. \quad (\text{A.3})$$

Using dimensionless parameters as defined in Table 1 and $\gamma = \lambda t_0$ one obtains

$$\frac{\partial}{\partial \tau} \Lambda = -\eta_0 \sqrt{2} (\sin \chi \sin(\theta) q_A + \cos \chi \sin(\theta + \beta) q_B) - \gamma \Lambda, \quad (\text{A.4})$$

which is identical to equation (3a).

Equation (3b) is obtained after dividing Eq. (A.2) by I / t_0 .

Appendix B. Macroscopic realization of the mean field equations

According to equations (1a) and (1b), the charge dynamics inside an island is determined by

$$\dot{Q} = W_{\text{in}}(\theta') (Q_{\max} - Q) - W_{\text{out}}(\theta') Q, \quad (\text{B.1})$$

where Q is the charge on the island with maximum value Q_{\max} and $W_{\text{in/out}}$ are periodic functions of θ' of the form

$$W_{\text{in}}(\theta') = \frac{1}{t_0} e^{-\xi \cos \theta'}, \quad (\text{B.2})$$

$$W_{\text{out}}(\theta') = \frac{1}{t_0} e^{\xi \cos \theta'}. \quad (\text{B.3})$$

One could think of realizing Eq. (B.1) by using a RC circuit with two capacitors with capacitances C_{in} and C_{out} configured in series

$$V = R \dot{Q} + Q \left(\frac{1}{C_{\text{in}}} + \frac{1}{C_{\text{out}}} \right) = R \dot{Q} + Q \left(\frac{C_{\text{in}} + C_{\text{out}}}{C_{\text{in}} C_{\text{out}}} \right), \quad (\text{B.4})$$

where V is the voltage of the circuit and $C = (C_{\text{in}} + C_{\text{out}}) / (C_{\text{in}} C_{\text{out}})$ is the effective capacitance. Comparing Eqs. (B.1) and (B.4) one obtains

$$W_{\text{in}}(\theta') = \frac{1}{C_{\text{in}}(\theta') R}, \quad (\text{B.5})$$

$$W_{\text{out}}(\theta') = \frac{1}{C_{\text{out}}(\theta') R}, \quad (\text{B.6})$$

or

$$C_{\text{in}}(\theta') = \frac{t_0}{R} e^{-\xi \cos \theta'}, \quad (\text{B.7})$$

$$C_{\text{out}}(\theta') = \frac{t_0}{R} e^{\xi \cos \theta'}. \quad (\text{B.8})$$

Finally, the voltage also has an angular dependence, namely

$$V(\theta') = \frac{Q_{\text{max}}}{C_{\text{in}}(\theta')}. \quad (\text{B.9})$$

- [1] Wesley R. Browne and Ben L. Feringa. Making molecular machines work. *Nat. Nanotechnol.*, 1(1):25–35, 2006.
- [2] Euan R. Kay, David A. Leigh, and Francesco Zerbetto. Synthetic Molecular Motors and Mechanical Machines. *Angew. Chemie Int. Ed.*, 46(1-2):72–191, January 2007.
- [3] Kwanoh Kim, Jianhe Guo, Xiaobin Xu, and Donglei Emma Fan. Micromotors with Step-Motor Characteristics by Controlled Magnetic Interactions among Assembled Components. *ACS Nano*, 9(1):548–554, jan 2015.
- [4] Jianhe Guo, Kwanoh Kim, Kin Wai Lei, and D. L. Fan. Ultra-durable rotary micromotors assembled from nanoentities by electric fields. *Nanoscale*, 7(26):11363–11370, 2015.
- [5] Claudio Maggi, Filippo Saglimbeni, Michele Dipalo, Francesco De Angelis, and Roberto Di Leonardo. Micromotors with asymmetric shape that efficiently convert light into work by thermocapillary effect. *Nat. Commun.*, 6:1–5, 2015.
- [6] Nagatoshi Koumura, Robert W. J. Zijlstra, Richard A. van Delden, Nobuyuki Harada, and Ben L. Feringa. Light-driven monodirectional molecular rotor. *Nature*, 401(6749):152–155, 1999.
- [7] T. R. Kelly, H. De Silva, and R. A. Silva. Unidirectional rotary motion in a molecular system. *Nature*, 401(6749):150–152, 1999.
- [8] S. W. D. Bailey, I. Amanatidis, and C. J. Lambert. Carbon Nanotube Electron Windmills: A Novel Design for Nanomotors. *Phys. Rev. Lett.*, 100(25):256802, 2008.
- [9] Raúl Bustos-Marín, Gil Refael, and Felix von Oppen. Adiabatic Quantum Motors. *Phys. Rev. Lett.*, 111(6):060802, 2013.
- [10] Jean-François Morin, Yasuhiro Shirai, and James M. Tour. En route to a motorized nanocar. *Org. Lett.*, 8(8):1713–1716, 2006.
- [11] Alexander Croy and Alexander Einfeld. Dynamics of a nanoscale rotor driven by single-electron tunneling. *EPL (Europhysics Lett.)*, 98(6):68004, 2012.
- [12] Boyang Wang, Lela Vuković, and Petr Král. Nanoscale rotary motors driven by electron tunneling. *Phys. Rev. Lett.*, 101(18):186808, 2008.
- [13] Anatoly Smirnov, Lev Murokh, Sergey Savel'ev, and Franco Nori. Bio-mimicking rotary nanomotors. In *SPIE Eur. Microtechnologies New Millenn.*, volume 7364, pages 73640D—73640D. International Society for Optics and Photonics, 2009.
- [14] David A. Leigh, Jenny K. Y. Wong, François Dehez, and Francesco Zerbetto. Unidirectional rotation in a mechanically interlocked molecular rotor. *Nature*, 424(6945):174–179, 2003.
- [15] A. M. Fennimore, T. D. Yuzvinsky, Wei-Qiang Han, M. S. Fuhrer, J. Cumings, and A. Zettl. Rotational actuators based on carbon nanotubes. *Nature*, 424(6947):408–410, jul 2003.
- [16] Richard A. van Delden, Matthijs K. J. ter Wiel, Michael M. Pollard, Javier Vicario, Nagatoshi Koumura, and Ben L. Feringa. Unidirectional molecular motor on a gold surface. *Nature*, 437(7063):1337–1340, oct 2005.
- [17] U. G. E. Perera, F. Ample, H. Kersell, Y. Zhang, G. Vives, J. Echeverria, M. Grisolia, G. Rapenne, C. Joachim, and S-W. Hla. Controlled clockwise and anticlockwise rotational switching of aÅmolecular motor. *Nat. Nanotechnol.*, 8(1):46–51, 2013.
- [18] Gregg S. Kottas, Laura I. Clarke, Dominik Horinek, and Josef Michl. Artificial molecular rotors. *Chem. Rev.*, 105(4):1281–1376, 2005.
- [19] Maria Guix, Carmen C. Mayorga-Martinez, and Arben Merkoçi. Nano/Micromotors in (Bio)chemical Science Applications. *Chem. Rev.*, 114(12):6285–6322, jun 2014.

- [20] Colin J. Murphy and E. Charles H. Sykes. Development of an Electrically Driven Molecular Motor. *Chem. Rec.*, 14(5):834–840, 2014.
- [21] Puneet Mishra, Jonathan P. Hill, Saranyan Vijayaraghavan, Wim Van Rossom, Shunsuke Yoshizawa, Maricarmen Grisolia, Jorge Echeverria, Teruo Ono, Katsuhiko Ariga, Tomonobu Nakayama, Christian Joachim, and Takashi Uchihashi. Current-Driven Supramolecular Motor with In Situ Surface Chiral Directionality Switching. *Nano Lett.*, 15(7):4793–4798, jul 2015.
- [22] Tibor Kudernac, Nopporn Ruangsapichat, Manfred Parschau, Beatriz Maciá, Nathalie Katsonis, Syuzanna R. Harutyunyan, Karl-Heinz Ernst, and Ben L. Feringa. Electrically driven directional motion of a four-wheeled molecule on a metal surface. *Nature*, 479(7372):208–211, 2011.
- [23] Rienk Eelkema, Michael M. Pollard, Javier Vicario, Nathalie Katsonis, Blanca Serrano Ramon, Cees W. M. Bastiaansen, Dirk J. Broer, and Ben L. Feringa. Molecular machines: Nanomotor rotates microscale objects. *Nature*, 440(7081):163–163, 2006.
- [24] Jiaobing Wang and Ben L. Feringa. Dynamic Control of Chiral Space in a Catalytic Asymmetric Reaction Using a Molecular Motor. *Science*, 331(6023):1429–1432, mar 2011.
- [25] Stephen P. Fletcher, Frédéric Dumur, Michael M. Pollard, and Ben L. Feringa. A reversible, unidirectional molecular rotary motor driven by chemical energy. *Science*, 310(5745):80–82, oct 2005.
- [26] A. J. Lichtenberg and M. A. Lieberman. *Regular and Chaotic Dynamics*, volume 38 of *Applied Mathematical Sciences*. Springer New York, New York, NY, 1992.
- [27] Ying-Cheng Lai and Tamás Tél. *Transient Chaos*, volume 173 of *Applied Mathematical Sciences*. Springer New York, New York, NY, 2011.